Dalton Transactions

ROYAL SOCIETY OF CHEMISTRY

PAPER

View Article Online
View Journal | View Issue

Cite this: *Dalton Trans.*, 2024, **53**, 11344

The synergistic interplay of hierarchy, crystal size, and Ga-promotion in the methanol-to-aromatics process over ZSM-5 zeolites†

Kun Liu,‡[a] Tuiana Shoinkhorova,‡[b] Xinyu You, ‡[a] Xuan Gong,[a,b] Xin Zhang,[a] Sang-Ho Chung,[b] Javier Ruiz-Martínez, *[b] Jorge Gascon *[b] and Abhishek Dutta Chowdhury *[a]

In the context of advancing social modernization, the projected shortfall in the demand for renewable aromatic hydrocarbons is expected to widen, influenced by industries like high-end materials, pharmaceuticals, and consumer goods. Sustainable methods for aromatic production from alternative sources, particularly the methanol-to-aromatics (MTA) process using zeolite ZSM-5 and associated with the "methanol economy", have garnered widespread attention. To facilitate this transition, our project consolidates conventional strategies that impact aromatics selectivity—such as using hierarchical zeolites, metallic promoters, or altering zeolite physicochemical properties—into a unified study. Our findings demonstrate the beneficial impact of elongated crystal size and heightened zeolite hierarchy on preferential aromatics selectivity, albeit through distinct mechanisms involving the consumption of shorter olefins. While metallic promoters enhance MTA performance, crystal size, and hierarchy remain pivotal in achieving the maximized aromatics selectivity. This study contributes to a deeper understanding of achieving superior aromatics selectivity through physicochemical modifications in zeolite ZSM-5 during MTA catalysis, thereby advancing the field's comprehension of structure–reactivity relationships.

Received 16th March 2024,
Accepted 13th June 2024

DOI: 10.1039/d4dt00793j

rsc.li/dalton

1. Introduction

The direct accessibility of aromatics-based petrochemicals from non-petroleum-based resources is considered to be one of the significant challenges of our time in the chemical industry.[1] Aromatic hydrocarbons, with a particular emphasis on benzene, toluene, and xylene (BTX), serve as essential raw materials in contemporary pharmaceuticals, fragrances, and, notably, the polymer industry.[1–5] Due to enhanced scrutiny of carbon emissions and more stringent environmental regulations, the scientific community has been compelled to investigate alternative, renewable pathways for producing aromatics-based hydrocarbons. Consequently, there has been a notable focus recently on the methanol-to-aromatics (MTA) process utilizing zeolite ZSM-5 as a catalyst.[1–3,6–10] The MTA is a sister reaction of the zeolite-catalyzed methanol-to-hydrocarbons (MTH) process.[11–20] Should methanol be derived from diverse sustainable sources like waste, biomass, and even CO_2, the entire technology would become renewable, aligning with the concept of a "methanol economy".[11,21–26] Hence, relying on the MTA process driven by sustainably sourced methanol emerges as our most promising strategy to meet the future demands for renewable aromatics/BTX species (Fig. 1).[1–4,8]

The zeolite-catalyzed MTH process was primarily popular over the zeolite ZSM-5 (MFI topology, 10-member ring, MR) and zeo-type SAPO-34 (CHA topology, 8MR) materials.[13–15,20,27–29] Similar to any process catalyzed by zeolites, ensuring "shape selectivity" is a crucial factor in governing product specificity.[12,16–18,30] For instance, in the existing industrial methanol-to-olefins (MTO) process, zeo-type SAPO-34 is employed, leveraging its smaller pores to produce the desired shorter olefins.[14,15,19,20,31,32] In the pursuit of facilitating aromatics production, our reliance should be on zeolites with >8 MR pores. However, larger pore zeolites (12 MR, such as Beta Zeolite) are unsuitable as they accelerate catalyst deactivation.[21,33] Therefore, the zeolite-catalyzed MTA processes were predominantly reported over 10 MR zeolites, especially ZSM-5, because its wider straight channel of ZSM-5 promotes aromatization by providing the right

[a]*College of Chemistry and Molecular Sciences, Wuhan University, Wuhan, Hubei, 430072, PR China. E-mail: abhishek@whu.edu.cn*
[b]*KAUST Catalysis Center (KCC), King Abdullah University of Science and Technology (KAUST), Thuwal 23955, Saudi Arabia. E-mail: javier.ruizmartinez@kaust.edu.sa, jorge.gascon@kaust.edu.sa*

†Electronic supplementary information (ESI) available. See DOI: https://doi.org/10.1039/d4dt00793j

‡These authors contributed equally.

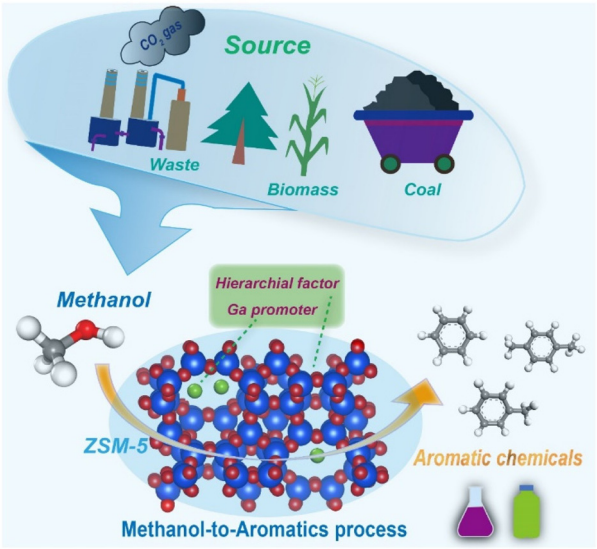

Fig. 1 The big picture: the efficacy of the MTA process over the zeolite ZSM-5 has been evaluated with respect to the crystal size, hierarchy, and Ga-promotion.

confinement.[18,34,35] Given that these aromatics also serve as precursors for coke, achieving a durable catalyst lifetime without compromising preferential aromatics selectivity presents an additional technical challenge. To overcome this limitation, the catalysis community employed multiple strategies, like using hierarchical zeolites,[36–41] adding a metallic promoter (*e.g.*, Zn[2,7–9,39,42–44] or Ga[4,10,36,45]), and altering the physicochemical properties of zeolites.[1,37,46–48] Each of these research strategies has a beneficial impact on MTA performance to some extent, albeit maximizing aromatics selectivity remained a challenge.

In our endeavor to enhance the crucial factors influencing aromatics selectivity in the MTA process, we have formulated this project, consolidating all previously employed strategies into a unified system or study. We believe this research approach will elevate the structure–reactivity understanding of MTA chemistry. For instance, in attempting to establish a comprehensive knowledge of MTA catalysis over zeolite ZSM-5 (see Table S1†),[7–10,36–50] the understanding surrounding the morphology, crystal size, and introduction of hierarchical porosity in zeolites/zeolite carriers and their catalytic relevance is inherently contentious. The different research groups have reported that superior aromatic selectivity was achieved during the MTA process over nano-sized hierarchical ZSM-5,[46] small crystallite Zn/H-ZSM-5,[51,52] and hollow Zn/ZSM-5 zeolites.[6,53] Conversely, some studies have underscored the positive influence of nano-sized hierarchical ZSM-5 on propylene/C_2–C_4 olefins selectivity (the primary products of alkene cycle).[54–58] However, these small olefin fractions could be consumed over the elongated zeolite crystals, in principle, leading to aromatics formation by simply tuning the physicochemical properties. This aspect represents one of the scopes of the current study. To bridge this knowledge gap, we have conceived this project, systematically manipulating both crystal size and hierarchy under similar acidity conditions, both in the presence and absence of Ga-promoters, to comprehend their collective impact on MTA catalysis.

In this study, we initially synthesized three core zeolite ZSM-5 variants with uniform acidity but variable crystal sizes and hierarchical properties: (i) nanosized, spherical, and purely microporous ZSM-5, (ii) hexagonal prismatic and hierarchical ZSM-5, and (iii) coffin-shaped and hierarchical ZSM-5. The non-surfactant and environmentally friendly hard template glucose was used to deliver hierarchical zeolites with varying crystal sizes under identical acidic properties to establish the interplay mechanism between crystal size (coffins and hexagonal bars) and hierarchy in MTA catalysis.[58,59] Herein, coffin-shaped and elongated particle-sized hierarchical ZSM-5 zeolites delivered superior aromatics selectivity (up to 22% as compared to 15% over microporous nano-sized zeolite) over its counterparts under our MTA reaction conditions (Reaction temperature = 400 °C, WHSV = 4 h^{-1}, 1 bar). Subsequently, all the synthesized zeolites underwent Ga impregnation in equal amounts to enhance aromatics production. Once again, the Ga-promoted hierarchical ZSM-5 zeolites with a coffin-shaped morphology and elongated crystal size demonstrated superior performance compared to the other catalysts used in this study (aromatics selectivity up to 34%, including 73% of BTX fraction). Traditional characterization tools were employed to elucidate the catalytic performance, revealing that higher consumption of shorter olefins over elongated zeolite crystals is pivotal for achieving superior aromatics selectivity. Notably, both crystal size and hierarchy contribute to aromatics production, especially in the BTX fraction, but in distinct ways: the consumption of olefins and the enhancement of aromatics exhibit a linear relationship with hierarchical properties, while they demonstrate an exponential relationship with crystal size, both in the presence and absence of Ga-promoters. In essence, this study provides insights and evidence on how manipulating crystal size, introducing hierarchical porosity, and incorporating Ga promoters impact MTA catalysis over medium-acidic ZSM-5 zeolite. This knowledge contributes to a better understanding of achieving superior aromatic selectivity in the MTA process.

2. Results and discussion

2.1. Synthesis and characterization

This work aimed to establish the complicated structure–reactivity relationships within the methanol-to-aromatics (MTA) chemistry over the zeolite ZSM-5, considering the following parameters: (i) the impact of Ga-promoter combined with (ii) crystal sizes, and (iii) hierarchical pores. It involved the synthesis of two sets of zeolites. The first set involved the controlled addition of glucose as a hard template to synthesize three different crystal morphologies and physicochemical properties of ZSM-5 zeolites: (i) nanosized, spherical, and purely microporous ZSM-5 (m-ns), (ii) hexagonal prismatic and hierarchical ZSM-5 (h-hexag), and (iii) coffin-shaped and hierarchi-

Table 1 Summary of representative physicochemical properties of zeolites used in this work

Catalysts	Si/Al ratio[a]	Specific surface area[b] (m^2 g^{-1})			Pore volume[b] (cm^3 g^{-1})			HF[c]	Size[d] (nm)
		Total	Micro	External	V_{total}	V_{micro}	V_{meso}		
ZSM-5 (m-ns)	103	393	372	21	0.24	0.19	0.05	0.04	110
ZSM-5 (h-hexag)	108	443	325	118	0.35	0.17	0.18	0.13	450
ZSM-5 (h-coffin)	113	458	302	156	0.37	0.16	0.21	0.15	4600
Ga/ZSM-5 (m-ns)	107	342	330	12	0.19	0.14	0.05	0.03	—
Ga/ZSM-5 (h-hexag)	111	413	309	104	0.32	0.15	0.17	0.12	—
Ga/ZSM-5 (h-coffin)	119	428	304	124	0.34	0.14	0.20	0.13	—

[a] The Si/Al ratios of three ZSM-5 zeolites were calculated by XRF (Si, Al), refer to Table S2.† [b] Calculated based on Ar-BET results. [c] Hierarchical factor (HF) defined as $(S_{External}/S_{BET}) \times (V_{mic}/V_{total})$.[39,58,59,65] [d] Determined by Nanomeasure software based on the TEM images of all synthesized zeolites (refer to Fig. S1†).

cal ZSM-5 (h-coffin) with reduced thickness along the *b*-axis.[58,59] The ZSM-5 (h-hexag) and ZSM-5 (h-coffin) zeolites modified with glucose, exhibited hierarchical pore structure, while the terms 'm' and 'h' represented purely microporous and hierarchical natures, respectively. All three zeolites shared identical initial gel composition and synthesis methods, except for adding glucose and water and adjusting aging steps, ensuring their Si/Al ratios remained around 110 (Table 1). The second set involved impregnating an equal amount of Ga $(NO_3)_3$ onto the three parent zeolites to ensure approximately 2 wt% of Ga (Table S2†). The resulting Ga-modified ZSM-5 zeolites were named Ga/ZSM-5 (m-ns), Ga/ZSM-5 (h-hexag), and Ga/ZSM-5 (h-coffin), corresponding to the three respective parent zeolites. We refer to the "Materials and methods" section in the ESI† for more synthetic details (also refer to Fig. 2 and Table S2†).

Subsequently, the crystal structures of all synthesized zeolites were characterized using XRD. The XRD patterns demonstrated excellent crystallinity in all synthesized zeolites (Fig. 3). Comparison with the standard card JCPDS (44-0003) for ZSM-5 zeolite revealed characteristic diffraction peaks near 2θ at 7.9°, 8.8°, 23.1°, 23.8°, and 24.4°,[21] indicating the presence of ZSM-5 zeolite features with pure phase in all synthesized zeolites.[21,56,58] Furthermore, these zeolites exhibited orthorhombic symmetry (*Pnma*).[58,59] Relative crystallinity and the symmetry of characteristic diffraction peaks remained almost unchanged in the three impregnated Ga/ZSM-5 zeolite materials. Moreover, no peaks related to Ga clusters/species or splitting peaks due to Ga replacing framework T atoms were detected in the XRD patterns, implying no change of orthorhombic symmetry.[60] This suggested that the obtained Ga loading resulted in a high dispersion of Ga clusters/species within the channels of the parent ZSM-5 zeolites.[4,7,10,36] These outcomes aligned with the characteristics of the impregnation method and were expected to exclude any interference caused by the introducing method of Ga and the discrepancy in loading amounts (Table S2†).

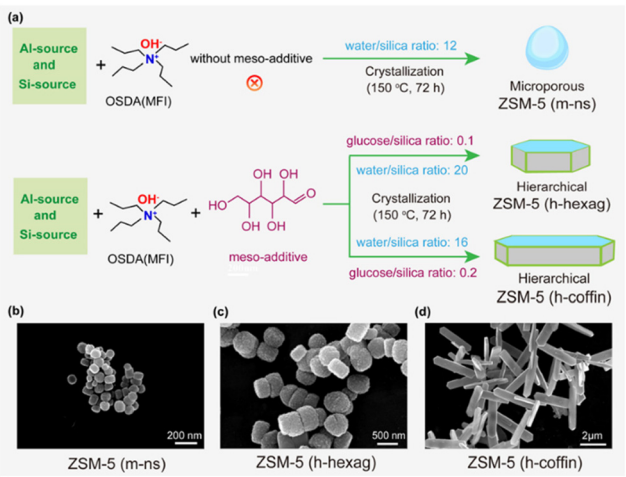

Fig. 2 (a) Synthesis schemes of ZSM-5 zeolites with non-identical physicochemical properties using glucose as the hard template. The principal distinctions among the respective synthesis methods stem from the quantities of water and glucose utilized, resulting in varying particle sizes. (b–d) TEM images of three synthesized ZSM-5 zeolites: (b) ZSM-5 (m-ns), (c) ZSM-5 (h-hexag), and (d) ZSM-5 (h-coffin) zeolites.

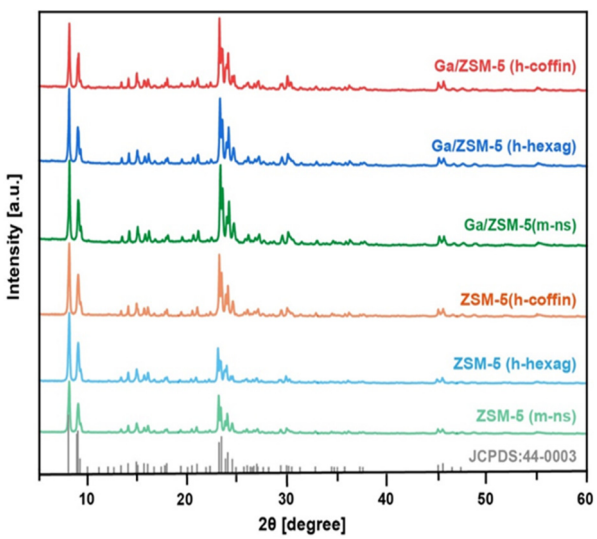

Fig. 3 X-ray diffraction (XRD) patterns of synthesized ZSM-5 (m-ns), ZSM-5 (h-hexag), ZSM-5 (h-coffin), Ga/ZSM-5 (m-ns), Ga/ZSM-5 (h-hexag) and Ga/ZSM-5 (h-coffin) zeolites.

TEM images indicated significant variations in the morphology and particle size of the zeolite with changes in the amount of glucose, the mesoporous templating agent, and water during aging steps (Fig. 2(b–d)). The ZSM-5 (m-ns) zeolite displayed a spherical shape with a crystal size of approximately 110 nm (Fig. S1†). ZSM-5 (h-hexag) exhibited a hexagonal morphology, with a crystal size of around 450 nm (Fig. S1†). ZSM-5 (h-coffin) presented a coffin-shaped morphology, with a crystal size of approximately 4.6 μm (*c*-axis) and about 0.21 μm (*b*-axis) (Fig. S1†). This aspect confirmed the effectiveness of the tailored synthesis strategy for controlling zeolite crystal morphology.[58,59] Subsequently, the distribution of various elements on the catalyst surface was examined through elemental mapping by the high-resolution transmission electron microscope (HR-TEM). The elemental mapping images of TEM revealed that upon loading with Ga, the crystal morphology of the zeolite did not change compared to the corresponding parent ZSM-5 zeolite (Fig. 2(b–d) and Fig. S2†). Additionally, Ga clusters/species were highly dispersed without agglomeration, consistent with the results obtained from XRD analysis.

The Ar-physisorption characterization was employed to probe the surface area and pore properties of all synthesized zeolites (Fig. S3† and Table 1). From the desorption/adsorption isotherms of these synthesized zeolites, ZSM-5 (m-ns) and its derived Ga/ZSM-5 (m-ns) zeolites exhibited a typical type-I isotherm, indicating its microporous structure.[21,56,58] In contrast, the other four zeolites synthesized with the addition of glucose display an H_4-type hysteresis loop in the relative pressure range of P/P_0 = 0.4–0.9, indicating the hierarchical pore nature with the coexistence of micropores and mesopores in these zeolites.[56,60,61] Due to the relatively larger crystal size, the hierarchical pore-containing materials exhibited no pronounced hysteresis loop at higher relative pressures (P/P_0 = 0.8–1.0), indicating that intracrystalline mesopores might predominantly exist within the synthesized hierarchical zeolites.[56,60–63] As anticipated, the presence of mesopores in hierarchical zeolites resulted in a decrease in their micropore volume compared to microporous zeolites, accompanied by an increase in mesopore volume, total pore volume, and specific surface area (Table 1). Additionally, due to the relatively lower levels of Ga impregnation, the surface area and pore volume of the three Ga/ZSM-5 zeolites were generally close to their respective parent zeolites. The slight decrease in the total surface area and pore volume observed in these derived Ga/ZSM-5 zeolites might be attributed to the existence of Ga clusters/species within the zeolite channels.[2,10,36,64]

NH_3-TPD was conducted to assess the acid distribution of all as-synthesized ZSM-5 and Ga/ZSM-5 zeolites (Table S2 and Fig. S4†), which revealed the acid distribution changes caused by the introduction of Ga on the parent ZSM-5 zeolites. Typically, these zeolites exhibited three NH_3 desorption peaks at ≤200 °C, 200–300 °C, and ≥300 °C, which were classified as weak (WAS), medium (MAS), and strong acid sites (SAS), respectively.[21,56,66,67] Herein, the Ga/ZSM-5 zeolites exhibited medium acid sites to some extent and diminished stronger acidity. This aspect could be attributed to substituting some of the zeolite's Brønsted acids with Ga clusters/species, resulting in additional medium acidity.[7,8,12,37,68–70] Additionally, all three derived Ga/ZSM-5 zeolites exhibited a trend where the desorption peaks of SAS shifted towards lower temperatures (Fig. S4†), while those of WAS shifted towards higher temperatures compared to the parent non-promoted ZSM-5 zeolite. This aspect is attributed to the increased Lewis acidic strength of Ga/ZSM-5 zeolites. It is also interesting to note that due to the easier diffusion of 'trapped' ammonia molecules through mesopores, the desorption peak temperatures in the as-synthesized hierarchical zeolites were relatively lower compared to microporous zeolites (Fig. S4†).[8,56,68–70] Moreover, glucose-assisted synthesis of hierarchical zeolites led to more Al incorporation, *preferably* in the framework position, as confirmed by the simultaneous slight increase in Si/Al ratio and strong acid content (see Table S2†).[58,59] In general, changes in the hierarchy and further introduction of Ga led to alterations in the acid distribution. These acid-related properties of the zeolites collectively lay the foundation for further enhancing their MTA performance.[7,8,71]

Next, X-ray photoelectron spectroscopy (XPS) was employed to examine the Ga species within ZSM-5 zeolites further. When Ga was introduced *via* the impregnation method, it preferentially interacted with the Brønsted acid sites within the zeolite pores, replacing some of the hydroxyl H^+ at these sites.[36,45,72,73] Herein, upon calcination, a portion of the Ga^{2+} typically transforms into neutral and ionic Ga species in the forms of oxides and hydroxides. Here, similar XPS signals for Ga were observed on all our Ga-based zeolites: Ga $2p_{3/2}$ (Fig. S5,† 1116–1122 eV).[72,73–75] These signals can be deconvoluted to fit three species: Ga_2O_3 species (Ga(I)) on the zeolite surface, with a peak at ~1117.6 eV; tetrahedrally coordinated Ga(II) species in the zeolite framework, with a peak at ~1118.6 eV; and extra-framework Ga(III) species interacting with the zeolite framework, with a peak at ~1120.4 eV (see Fig. S5†).[72,73] This observation indicates that these materials exhibit a similar distribution of Ga species, with the majority entering the zeolite framework and existing as tetrahedrally coordinated Ga species after calcination. Notably, the content of surface Ga_2O_3 species correlates with crystal size (and/or HF), as reflected by the higher proportion of surface Ga_2O_3 (Ga(I)) species in Ga/ZSM-5 (h-coffin), which has the largest crystal size (~4.6 μm). This physicochemical property is expected to be closely related to their differences in catalytic performance. Since the introduced Ga species could neutralize the Brønsted acidity of zeolites to some extent, this aspect could correspond to the introduction of medium-strength Lewis acid sites (also see NH_3-TPD study, Fig. S4†). The introduction of Ga species and the resulting modification of acid site distribution within Ga/ZSM-5 zeolites can influence their overall catalytic performance. For instance, these changes can enhance the formation of certain intermediates (such as formaldehyde), reduce hydrogen transfer, and facilitate the oligomerization and cyclization/aromatization of short-chain olefins,[73–78] thereby consuming short-chain olefins and increasing the desired aromatics selectivity.

2.2. MTA catalytic performance evaluation

Next, all synthesized zeolites were subjected to MTA catalytic performance evaluation (reaction conditions: atmospheric pressure, reaction temperature = 400 °C, WHSV = 4 h^{-1}, see Fig. 4, 5 and Fig. S6 to S12†). After at least 16 hours of methanol feeding, none of the catalysts showed signs of any significant catalyst deactivation (*i.e.*, methanol conversion below 95%), indicating their durability in the catalytic MTA process (Fig. S6–S12†). Typically, compared to purely microporous zeolites (*i.e.*, m-ns), both hierarchical ZSM-5 zeolites showed an increase in aromatics selectivity (*i.e.*, for ZSM-5 (m-ns) *vs.* ZSM-5 (h-hexag) *vs.* ZSM-5 (h-coffin): 15% *vs.* 20% *vs.* 22%; TOS = 12 hours). Such an increase of aromatics selectivity appeared with the increase in the hierarchical factor (HF) and crystal size, which led to increased consumption of shorter olefins (*i.e.*, for ZSM-5 (m-ns) *vs.* ZSM-5 (h-hexag) *vs.* ZSM-5 (h-coffin): 45% *vs.* 36% *vs.* 35%). Interestingly, the selectivity towards BTX (*i.e.*, benzene, toluene, xylene) fraction within aromatics also showed an analogous increase (*i.e.*, for ZSM-5 (m-ns) *vs.* ZSM-5 (h-hexag) *vs.* ZSM-5 (h-coffin): 46% *vs.* 59% *vs.* 67%) (Fig. 4 and Table S3†). The trend of both increased aromatics selectivity and a higher proportion of BTX fraction resulting from hierarchy and crystal size aligns with the goal of developing advanced MTA catalysts.[1,2,4] It should be worth noting that our BTX fraction primarily comprises toluene and xylene, with the benzene content remaining in the ≤3% range.

Furthermore, the introduction of Ga enhanced the aromatics selectivity in all cases (Fig. 4(d) and Fig. S9–S11†). This effect synergizes with the impact of HF and crystal size induced by glucose-assisted synthesis of hierarchical zeolites. For instance, Ga/(h-hexag) and Ga/ZSM-5 (h-coffin) zeolites showed a more substantial enhancement in aromatics selectivity compared to the respective parent ZSM-5 zeolites (see Fig. 4(d), Ga/ZSM-5 (m-ns), Ga/ZSM-5 (h-hexag), and Ga/ZSM-5 (h-coffin), a relative increase of around 40%, 50%, and 54%, respectively). While the consumption ratio of olefin selectivity also showed a similar pattern, for example, Ga/ZSM-5 (h-hexag) and Ga/ZSM-5 (h-coffin) zeolites exhibited a higher proportion of decrease in olefin selectivity compared to their respective parent ZSM-5 zeolites (see Fig. 4(d), Ga/ZSM-5 (m-ns), Ga/ZSM-5 (h-hexag), and Ga/ZSM-5 (h-coffin), relative decrease of around 16%, 22%, and 26%, respectively).

In addition, the introduction of Ga, which leads to changes in acidity, is also a key factor in enhancing aromatic hydrocarbons's selectivity.[8,10,36,79] Specifically, the shift in acid distribution from strong acid sites to medium acid sites resulted in a synergy between Brønsted and Lewis acids (Fig. S4†). This synergy promoted the consumption of short-chain olefins primarily *via* oligomerization and cyclization/aromatization

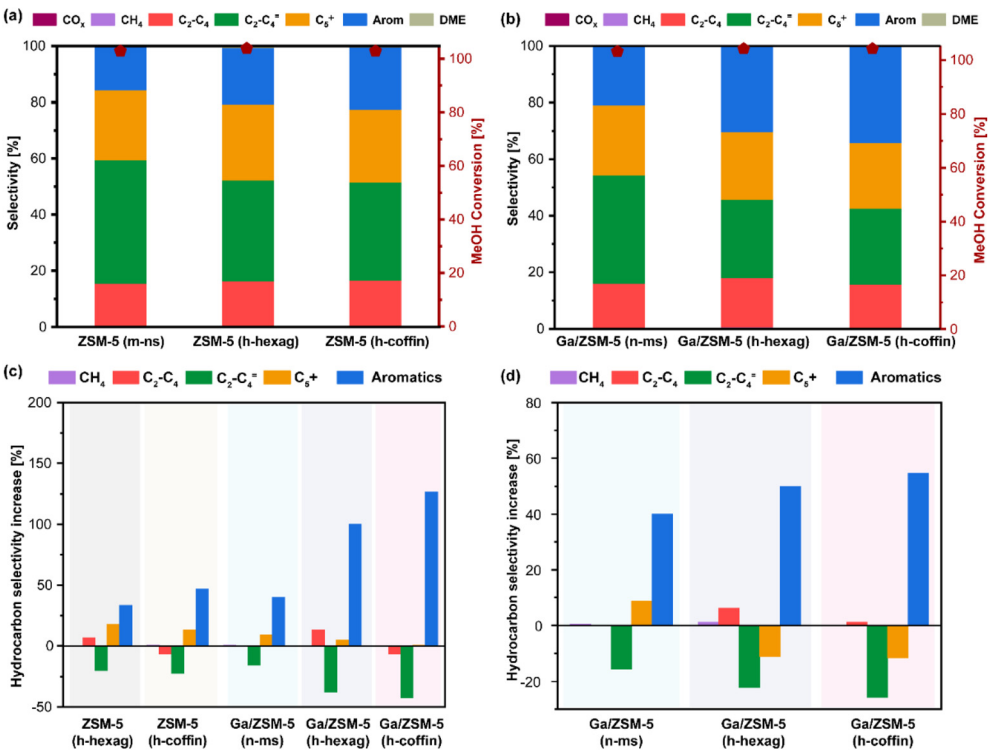

Fig. 4 Summary of the MTH catalytic test results: (a and b) hydrocarbon products selectivity and methanol conversion at time-on-stream of 12 hours (Reaction conditions: WHSV = 4 h^{-1}, Reaction temperature = 400 °C, Reaction pressure = 1 bar). The relative selectivity increase/decrease of key hydrocarbon products over five zeolites with respect to (c) parent ZSM-5 (m-ns) zeolite as well as (d) respective parent zeolites (*i.e.*, Ga/ZSM-5 *vs.* ZSM-5 series). Both referencing representations imply the enhancement of aromatics selectivity appeared at the expense of consuming short olefins.

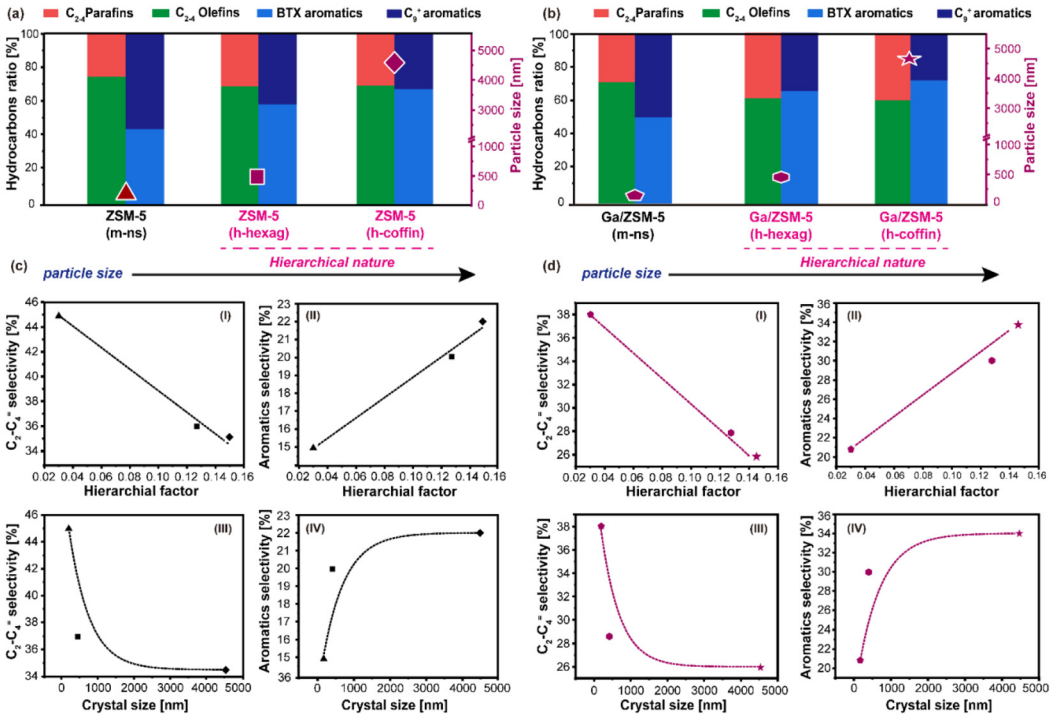

Fig. 5 (a and b) Relative hydrocarbon distribution of key products of (a) ZSM-5 (m-ns), ZSM-5 (h-hexag) and ZSM-5 (h-coffin) zeolites, and (b) Ga/ZSM-5 (m-ns), Ga/ZSM-5 (h-hexag) and Ga/ZSM-5 (h-coffin) zeolites. (c and d) Selectivity of C_2–C_4 olefins and aromatics as a function of hierarchical factor(HF) and crystal size. (The results based on time-on-stream (TOS) of 12 hours, WHSV = 4 h^{-1}, Reaction temperature = 400 °C, Reaction pressure = 1 bar). [triangle: ZSM-5 (m-ns), square: ZSM-5 (h-hexag), diamond: ZSM-5 (h-coffin), pentagon: Ga/ZSM-5 (m-ns), hexagon: Ga/ZSM-5 (h-hexag), star: Ga/ZSM-5 (h-coffin)].

processes, while inhibiting the further alkylation growth of BTX aromatics into C_{9+} aromatic species. These findings also highlighted the synergistic effectiveness of employing glucose-assisted zeolite synthesis protocol to tune the physicochemical properties: for example, the combination of having larger crystal size zeolites with hierarchy and the impact of Ga-promotion collectively led to superior MTA performance (~127% and ~59% relative increase in aromatics and BTX selectivity over Ga/ZSM-5 (h-coffin) as compared to ZSM-5 (m-ns) zeolite, see Fig. 4(c)). Interestingly, any other hydrocarbon selectivity did not alter much despite variations in the changes in aromatics selectivity and variation of physicochemical properties of zeolites (*e.g.*, ZSM-5 (m-ns) *vs.* Ga/ZSM-5 (h-coffin): ~15% *vs.* ~16% for C_2–C_4 paraffins and ~23% *vs.* ~23% C_{5+} paraffins, see Fig. 4 and Table S3†). This observation indicates the consumption of shorter olefins, promoted by the physicochemical properties of zeolites, is the key to accelerating BTX/aromatics selectivity in the current study. Furthermore, the hydrogen transfer process has not been significantly enhanced, which may be due to the combined effects of the changes in acid distribution and the specific forms of Ga species in Ga/ZSM-5 zeolites. In general, the consumption of short olefins (*via* oligomerization and cyclization/aromatization) appears to be more influenced by particle size variation than hydrogen-transfer activities.

By correlating the physicochemical properties of zeolites (*i.e.*, HF, crystal size) and key hydrocarbon product selectivity (Fig. 5), it can be inferred that the introduction of mesoporosity reduces the diffusion barrier for all product molecules and primarily contributes to the catalyst's durability.[39,41,57,58] Furthermore, longer crystal sizes prolong the diffusion path of olefinic species and, hence, facilitate their consumption to yield aromatics.[46] For instance, as-synthesized ZSM-5 (h-hexag) and ZSM-5 (h-coffin) zeolites exhibited increased crystal sizes and hierarchical factors compared to the nanosized ZSM-5 (m-ns) zeolite (see Table 1). These alterations correspond to relative increases in aromatics selectivity by ~33% and ~47%, respectively, and the relative decrease in olefins selectivity by ~20% and ~22%, respectively (Fig. 5(a)).

This trend was similarly reflected in Ga/ZSM-5 zeolite series: As compared to Ga/ZSM-5 (m-ns) zeolite, both Ga/ZSM-5 (h-hexag) and Ga/ZSM-5 (h-coffin) led to relative increases in aromatics selectivity by ~43% and ~62%, respectively, while the relative decrease in olefins selectivity by ~26% and ~32%, respectively (Fig. 5(b)). It has been observed that the key products selectivity changes in both the ZSM-5 and Ga/ZSM-5 zeolites followed a similar trend. In both instances, it is noteworthy that coffin-shaped crystals exhibited greater consumption of higher olefins and selectivity towards aromatics compared to their hexagonal counterparts. However, the HF values were fairly similar across all hierarchical zeolites used in this study (see Table 1). This observation has led us to understand that crystal size plays a more significant role than

HF in yielding higher preferential aromatics selectivity during MTA catalysis.

It is evident that both HF and crystal size was beneficial for catalysis, but in a non-identical way. For example, the selectivity of C_2–C_4 olefins and aromatics correlated linearly with the HF (Fig. 5(c)). In contrast, the selectivity of C_2–C_4 olefins and aromatics exhibited an exponential correlation with crystal size (Fig. 5(d)). Herein, we propose that olefins undergo gradual depletion along the diffusion pathways towards aromatization, reaching a threshold where the further increase in aromatic hydrocarbon selectivity becomes constrained by the larger crystal size (*e.g.*, from ZSM-5 (m-ns) (110 nm) to ZSM-5 (h-hexag) (450 nm), aromatics selectivity from 15% to 20%, while for ZSM-5 (h-coffin) (4600 nm), aromatics selectivity only to 22%). At the same time, HF assists in managing the diffusional dynamics of the catalyst, ensuring the system's durability by inhibiting deactivation. Collectively, all these combined factors (*e.g.*, crystal size, hierarchy, and Ga additive) promote the oligomerization of olefin molecules and further facilitate the aromatization process, consequently enhancing the selectivity towards aromatics, especially the BTX fraction.

2.3. Mechanistic outlook

While the above observation highlights the significant role of Ga in facilitating aromatization, it is essential to note that olefin consumption reaches a threshold with the increase in particle size, hindering further aromatization and thus limiting the additional increase in aromatics selectivity. Therefore, the consumption and oligomerization of shorter olefin appear to be more influenced by particle size, leading directly to alkylated aromatics *via* subsequent cyclization/aromatization, bypassing the need for further alkylation. As recently reported by multiple research groups independently,[67,73–78] besides the effects brought by the acid distribution characteristics, Ga-promoter could induce methanol dehydrogenation and disproportionation step to yield formaldehyde, which is considered a pivotal intermediate in the MTA process.[30,81] This intermediate could readily participate in hydrogen transfer, Prins reaction with dienes, and eventually promotes the catalyst deactivation.[67,79–81] This work demonstrates that processes involving formaldehyde are not significant promoting factors, likely due to the use of hierarchical medium-acidic zeolite. This is further confirmed by the relatively long catalytic lifespan and the low increase in the selectivity of C_2–C_4 alkanes (see Fig. 4 and S13†). The propylene/ethylene selectivity ratio was considered a pivotal descriptor measuring the extent of alkene and arene cycles in the MTH process, as ethylene was exclusively derived from the arene cycle.[11,30,82–89] Correspondingly, the Ga/ZSM-5 (h-coffin) zeolite, which exhibited the highest aromatic selectivity (~34%) under normal conditions, demonstrated the lowest propylene/ethylene ratio of 0.8. Conversely, the ZSM-5 (m-ns) zeolite, with the lowest aromatic selectivity (15%), displayed the highest propylene/ethylene ratio of 3.5 (Fig. S13†). These findings indicated that Ga-promoter and elongated particle size promoted the consumption of C_2–C_4 olefins to aromatics and significantly encouraged the arene cycle.[1–4,10,36,59] We integrated all the findings of this study into Fig. 6 to comprehensively illustrate the pivotal role of Ga in enhancing the catalytic MTA process over ZSM-5 zeolites, together with particle size and hierarchy factors.[58,59,72,73,90,91] The Ga-introduction led to the weakening of the cracking of C_{5+} hydrocarbons in the alkene cycle and promoted the oligomerization of shorter olefins to convert into aromatics. In addition, the Ga-induced disproportionation

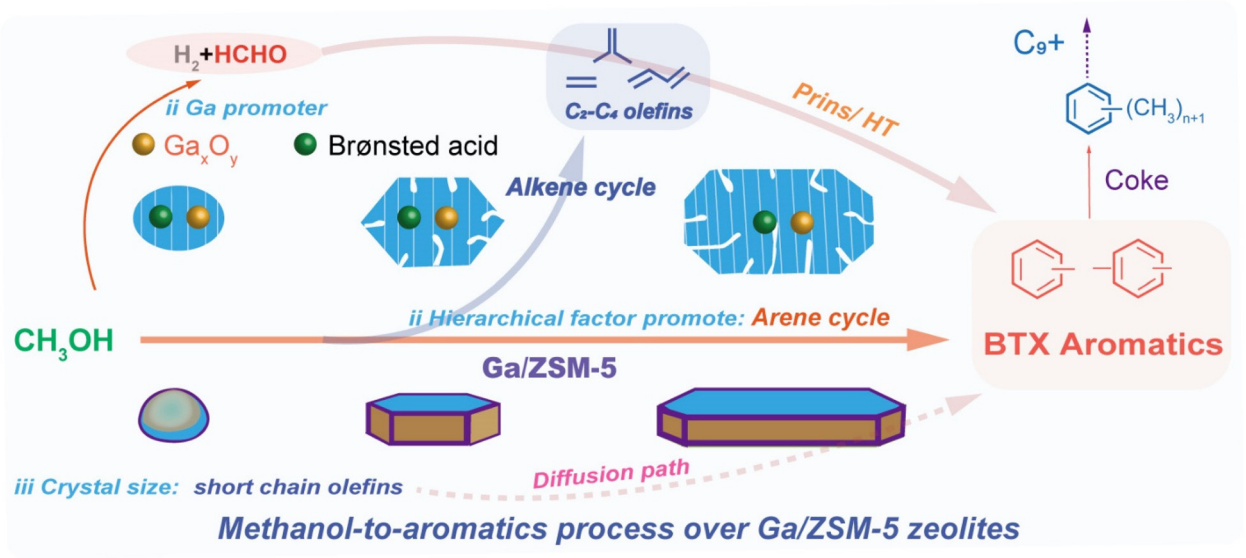

Fig. 6 The mechanistic overview summarizing the collective impact of Ga-promotion, particle size, and hierarchy to facilitating the aromatic products formation during the MTA process. Incorporating Ga could help the MTA process by promoting the production of formaldehyde intermediates, inhibiting C_{5+}-paraffins cracking, and promoting C_2–C_4 olefins oligomerization. In addition to Ga-promotion, the crystal size, and hierarchy of the zeolite also enhance aromatics production *via* strengthening the arene cycle in the dual-cycle process.

product of methanol (*i.e.*, formaldehyde) might also facilitate such aromatics production, confirming the synergistic effects between Ga, zeolite hierarchy, and crystal size in facilitating aromatic production.

3. Conclusions

Developing MTA catalysts with high performance and resistance to deactivation is pivotal for advancing sustainable technologies in aromatic hydrocarbon production, meeting the increasing demand for consumer goods and high-end materials in modern society, with a particular focus on enhancing BTX selectivity. To attain this goal, we have systematically examined three key aspects of zeolite catalysis that enhance aromatics production: crystal size, hierarchical nature, and metallic promoters. For a meaningful comparison of catalytic performance, we synthesized three core zeolites ZSM-5 with consistent acidity but differing crystal sizes and hierarchical properties: (i) nanosized, spherical, and purely microporous ZSM-5 (m-ns), (ii) hexagonal prismatic and hierarchical ZSM-5 (h-hexag), and (iii) coffin-shaped and hierarchical ZSM-5 (h-coffin). In the synthesis process, we employed a non-surfactant and environmentally friendly hard template, glucose, to yield hierarchical zeolites with varying crystal sizes and hierarchical properties under uniform acidic conditions. Herein, coffin-shaped hierarchical ZSM-5 zeolite, with elongated crystal size, delivered superior aromatics selectivity (22%) over its counterparts (nano spherical ZSM-5 zeolite: 15%) under our MTA reaction conditions. Upon Ga-promotion, the analogous Ga-promoted hierarchical zeolite with a coffin-shaped morphology demonstrated superior performance (aromatics selectivity: 34%, including 73% of BTX fraction) compared to the other catalysts used in this study.

We illustrate that achieving superior aromatics selectivity is contingent on a higher consumption of shorter olefins over elongated zeolite crystals. Significantly, both crystal size and hierarchy play roles in aromatics production, particularly in the BTX fraction, but in differing manners: the consumption of olefins and the increase in aromatics were mainly influenced by the crystal size parameter, whereas the hierarchy aids in enhancing catalyst durability by inhibiting deactivation. Hence, the optimal and synergistic benefits derived from particle size, hierarchical structure, and Ga promotion are crucial for facilitating MTA catalysis, particularly in promoting the formation of toluene and xylene. As a result, a deeper and more comprehensive understanding of attaining superior aromatics selectivity has been gained by manipulating the physicochemical properties of zeolite ZSM-5 during MTA catalysis. The thorough investigation of this process has provided insights into the intricacies of enhancing the selectivity of aromatics, shedding light on how the modification of zeolite characteristics influences the outcome of the MTA reaction. This enhanced understanding is crucial for advancing the design and development of more efficient MTA catalysts, particularly in terms of achieving targeted aromatics selectivity, a critical factor in the sustainable production of aromatic hydrocarbons.

Author contributions

These authors contributed equally: Kun Liu, Tuiana Shoinkhorova, and Xinyu You. Kun Liu: investigation, methodology, validation, formal analysis, writing – original draft. Tuiana Shoinkhorova: investigation, methodology, validation, formal analysis. Xinyu You: formal analysis, data curation, writing – original draft, writing – review & editing. Xuan Gong: investigation, formal analysis, writing – original draft. Xin Zhang: formal analysis, visualization, data curation. Sang-Ho Chung: investigation, validation, formal analysis, writing – review & editing. Javier Ruiz-Martínez: supervision, conceptualization, project administration, formal analysis, writing – review & editing, funding acquisition. Jorge Gascon: supervision, conceptualization, project administration, formal analysis, writing – review & editing, funding acquisition. Abhishek Dutta Chowdhury: conceptualization, supervision, project administration, formal analysis, writing – original draft, writing – review & editing, funding acquisition. All authors have given approval to the final version of the manuscript.

Conflicts of interest

There are no conflicts to declare.

Acknowledgements

This project has been financially supported by the King Abdullah University of Science and Technology (KAUST, URF/1/4406-01) and the National Natural Science Foundation of China (NSFC) (Grant No. 22350610243).

References

1 T. Shoinkhorova, T. Cordero-Lanzac, A. Ramirez, S. H. Chung, A. Dokania, J. Ruiz-Martinez and J. Gascon, *ACS Catal.*, 2021, **11**, 3602–3613.
2 Q. Gong, T. Fang, Y. Xie, R. Zhang, M. Liu, F. Barzagli, J. Li, Z. Hu and Z. Zhu, *Ind. Eng. Chem. Res.*, 2021, **60**, 1633–1641.
3 T. Li, T. Shoinkhorova, J. Gascon and J. Ruiz-Martinez, *ACS Catal.*, 2021, **11**, 7780–7819.
4 Z. Li, A. W. Lepore, M. F. Salazar, G. S. Foo, B. H. Davison, Z. Wu and C. K. Narula, *Green Chem.*, 2017, **19**, 4344–4352.
5 Z. Xi, B. Zhou, B. Jiang, J. Wang, Z. Liao, Z. Huang and Y. Yang, *Mol. Catal.*, 2019, **475**, 110493.
6 Z. Chen, Y. Ni, Y. Zhi, F. Wen, Z. Zhou, Y. Wei, W. Zhu and Z. Liu, *Angew. Chem.*, 2018, **130**, 12729–12733.

7 N. Wang, J. Li, W. Sun, Y. Hou, L. Zhang, X. Hu, Y. Yang, X. Chen, C. Chen, B. Chen and W. Qian, *Angew. Chem., Int. Ed.*, 2022, **61**, 10.
8 T. Fu, C. Cao, L. Zhang, L. Zhang, Q. Ma, Z. Xu, R. Wang, H. Li and Z. Li, *Ind. Eng. Chem. Res.*, 2023, **62**, 1865–1876.
9 I. Pinilla-Herrero, E. Borfecchia, T. Cordero-Lanzac, U. V. Mentzel, F. Joensen, K. A. Lomachenko, S. Bordiga, U. Olsbye, P. Beato and S. Svelle, *J. Catal.*, 2021, **394**, 416–428.
10 C. Liu, E. A. Uslamin, E. Khramenkova, E. Sireci, L. T. L. J. Ouwehand, S. Ganapathy, F. Kapteijn and E. A. Pidko, *ACS Catal.*, 2022, **12**, 3189–3200.
11 I. Yarulina, A. D. Chowdhury, F. Meirer, B. M. Weckhuysen and J. Gascon, *Nat. Catal.*, 2018, **1**, 398–411.
12 C. Li, C. Paris, J. Martínez-Triguero, M. Boronat, M. Moliner and A. Corma, *Nat. Catal.*, 2018, **1**, 547–554.
13 X. Wu, Y. Wei and Z. Liu, *Acc. Chem. Res.*, 2023, **56**, 2001–2014.
14 P. Tian, Y. Wei, M. Ye and Z. Liu, *ACS Catal.*, 2015, **5**, 1922–1938.
15 W. Zhang, S. Lin, Y. Wei, P. Tian, M. Ye and Z. Liu, *Natl. Sci. Rev.*, 2023, **10**(9), nwad120.
16 U. Olsbye, S. Svelle, M. Bjrgen, P. Beato, T. V. W. Janssens, F. Joensen, S. Bordiga and K. P. Lillerud, *Angew. Chem., Int. Ed.*, 2012, **51**, 5810–5831.
17 Y. Chai, W. Dai, G. Wu, N. Guan and L. Li, *Acc. Chem. Res.*, 2021, **54**, 2894–2904.
18 D. Fu, A. L. Paioni, C. Lian, O. van der Heijden, M. Baldus and B. M. Weckhuysen, *Angew. Chem., Int. Ed.*, 2020, **59**, 20024–20030.
19 M. Dusselier and M. E. Davis, *Chem. Rev.*, 2018, **118**, 5265–5329.
20 M. Yang, D. Fan, Y. Wei, P. Tian and Z. Liu, *Adv. Mater.*, 2019, **31**, 50.
21 X. You, X. Zhang, Y. Ye, H. Zhou, S. Jiang, X. Zhou and A. D. Chowdhury, *Dalton Trans.*, 2023, **52**, 15958–15967.
22 G. A. Olah, *Chem. Eng. News*, 2003, **81**, 5.
23 G. A. Olah, *Angew. Chem., Int. Ed.*, 2013, **52**, 104–107.
24 G. A. Olah, *Angew. Chem., Int. Ed.*, 2005, **44**, 2636–2639.
25 A. Goeppert, M. Czaun, J. P. Jones, G. K. Surya Prakash and G. A. Olah, *Chem. Soc. Rev.*, 2014, **43**, 7995–8048.
26 C. Filosa, X. Gong, A. Bavykina, A. D. Chowdhury, J. M. R. Gallo and J. Gascon, *Acc. Chem. Res.*, 2023, **56**, 3492–3503.
27 J. Liu, C. Zhang, Z. Shen, W. Hua, Y. Tang, W. Shen, Y. Yue and H. Xu, *Catal. Commun.*, 2009, **10**, 1506–1509.
28 Y. Wang, J. Han, N. Wang, B. Li, M. Yang, Y. Wu, Z. Jiang, Y. Wei, P. Tian and Z. Liu, *Chin. J. Catal.*, 2022, **43**, 2259–2269.
29 S. Müller, Y. Liu, M. Vishnuvarthan, X. Sun, A. C. Van Veen, G. L. Haller, M. Sanchez-Sanchez and J. A. Lercher, *J. Catal.*, 2015, **325**, 48–59.
30 X. Gong, Y. Ye and A. D. Chowdhury, *ACS Catal.*, 2022, **12**, 15463–15500.
31 X. Yuan, H. Li, M. Ye and Z. Liu, *AIChE J.*, 2019, **65**, 662–674.
32 E. Borodina, H. Sharbini Harun Kamaluddin, F. Meirer, M. Mokhtar, A. M. Asiri, S. A. Al-Thabaiti, S. N. Basahel, J. Ruiz-Martinez and B. M. Weckhuysen, *ACS Catal.*, 2017, **7**, 5268–5281.
33 Ø. Mikkelsen and S. Kolboe, *Microporous Mesoporous Mater.*, 1999, **29**, 173–184.
34 D. Fu, J. J. E. Maris, K. Stanciakova, N. Nikolopoulos, O. van der Heijden, L. D. B. Mandemaker, M. E. Siemons, D. S. Pastene, L. C. Kapitein, F. T. Rabouw, F. Meirer and B. M. Weckhuysen, *Angew. Chem., Int. Ed.*, 2022, **61**(5), e202114388.
35 A. Ramirez, X. Gong, M. Caglayan, S. A. F. Nastase, E. Abou-Hamad, L. Gevers, L. Cavallo, A. D. Chowdhury and J. Gascon, *Nat. Commun.*, 2021, **12**, 5914.
36 Y. Y. Chen, C. J. Chang, H. V. Lee, J. C. Juan and Y. C. Lin, *Ind. Eng. Chem. Res.*, 2019, **58**, 7948–7956.
37 C. Cheng, G. Li, D. Ji, Y. Zhao and J. Shen, *Microporous Mesoporous Mater.*, 2020, **299**, 110784.
38 A. Asghari, M. K. Khorrami and S. H. Kazemi, *Sci. Rep.*, 2019, **9**, 1.
39 X. Shen, J. Kang, W. Niu, M. Wang, Q. Zhang and Y. Wang, *Catal. Sci. Technol.*, 2017, **7**, 3598–3612.
40 N. Wang, W. Qian and F. Wei, *J. Mater. Chem. A*, 2016, **4**, 10834–10841.
41 H. Tian, Z. Chen, X. Yang, P. Gao, C. Jiao, F. Zha, Y. Chang and H. Chen, *Energy Fuels*, 2023, **37**, 14180–14191.
42 H. Tian, Z. Zhang and X. Ma, *Kinet. Catal.*, 2018, **59**, 618–627.
43 Y. Xin, P. Qi, X. Duan, H. Lin and Y. Yuan, *Catal. Lett.*, 2013, **143**, 798–806.
44 J. Qiao, J. Wang, A. I. Frenkel, J. Teng, X. Chen, J. Xiao, T. Zhang, Z. Wang, Z. Yuan and W. Yang, *RSC Adv.*, 2020, **10**, 5961–5971.
45 J. A. Lopez-Sanchez, M. Conte, P. Landon, W. Zhou, J. K. Bartley, S. H. Taylor, A. F. Carley, C. J. Kiely, K. Khalid and G. J. Hutchings, *Catal. Lett.*, 2012, **142**, 1049–1056.
46 L. Yang, Z. Liu, Z. Liu, W. Peng, Y. Liu and C. Liu, *Chin. J. Catal.*, 2017, **38**, 683–690.
47 Q. Ma, T. Fu, L. Yin and Z. Li, *Chem. Eng. J.*, 2023, **477**, 142252.
48 K. Wang, M. Dong, J. Li, P. Liu, K. Zhang, J. Wang and W. Fan, *Catal. Sci. Technol.*, 2017, **7**, 560–564.
49 Y. Zhang, Y. Qu, D. Wang, X. C. Zeng and J. Wang, *Ind. Eng. Chem. Res.*, 2017, **56**, 12508–12519.
50 M. Conte, J. A. Lopez-Sanchez, Q. He, D. J. Morgan, Y. Ryabenkova, J. K. Bartley, A. F. Carley, S. H. Taylor, C. J. Kiely, K. Khalid and G. J. Hutchings, *Catal. Sci. Technol.*, 2012, **2**, 105–112.
51 X. Niu, J. Gao, K. Wang, Q. Miao, M. Dong, G. Wang, W. Fan, Z. Qin and J. Wang, *Fuel Process. Technol.*, 2017, **157**, 99–107.
52 X. Niu, Y. Bai, Y. Du, H. Qi and Y. Chen, *R. Soc. Open Sci.*, 2022, **9**, 211284.
53 K. Wang, M. Dong, X. Niu, J. Li, Z. Qin, W. Fan and J. Wang, *Catal. Sci. Technol.*, 2018, **8**, 5646–5656.

54 Z. Wu, K. Zhao, Y. Zhang, T. Pan, S. Ge, Y. Ju, T. Li and T. Dou, *Ind. Eng. Chem. Res.*, 2019, **58**, 10737–10749.
55 H. Chen, Y. Wang, F. Meng, C. Sun, H. Li, Z. Wang, F. Gao, X. Wang and S. Wang, *Microporous Mesoporous Mater.*, 2017, **244**, 301–309.
56 X. You, X. Zhang, S. Jiang, Y. Ye, L. Gu, H. Zhou, P. Ma, J. Ftouni and A. D. Chowdhury, *Chin. J. Struct. Chem.*, 2024, **43**, 100265.
57 H. S. Kamaluddin, X. Gong, P. Ma, K. Narasimharao, A. D. Chowdhury and M. Mokhtar, *Mater. Today Chem.*, 2022, **26**, 101061.
58 K. Liu, M. Çağlayan, A. Dikhtiarenko, X. Zhang, O. Sayidov, E. Abou-Hamad, J. Gascon and A. D. Chowdhury, *Catal. Today*, 2023, **408**, 22–35.
59 K. Liu, A. Ramirez, X. Zhang, M. Çağlayan, X. Gong, J. Gascon and A. D. Chowdhury, *ChemSusChem*, 2023, **16**, e202300608.
60 S. V. Konnov, F. Dubray, E. B. Clatworthy, C. Kouvatas, J. P. Gilson, J. P. Dath, D. Minoux, C. Aquino, V. Valtchev, S. Moldovan, S. Koneti, N. Nesterenko and S. Mintova, *Angew. Chem., Int. Ed.*, 2020, **59**, 19553–19560.
61 C. Xing, G. Yang, M. Wu, R. Yang, L. Tan, P. Zhu, Q. Wei, J. Li, J. Mao, Y. Yoneyama and N. Tsubaki, *Fuel*, 2015, **148**, 48–57.
62 K. A. Cychosz, R. Guillet-Nicolas, J. García-Martínez and M. Thommes, *Chem. Soc. Rev.*, 2017, **46**, 389–414.
63 J. Li, S. Liu, H. Zhang, E. Lü, P. Ren and J. Ren, *Chin. J. Catal.*, 2016, **37**, 308–315.
64 M. Ghaedi and A. Izadbakhsh, *J. Fuel Chem. Technol.*, 2021, **49**, 1468–1486.
65 H. Chen, M. Yang, W. Shang, Y. Tong, B. Liu, X. Han, J. Zhang, Q. Hao, M. Sun and X. Ma, *Ind. Eng. Chem. Res.*, 2018, **57**, 10956–10966.
66 R. Martínez-Franco, Z. Li, J. Martínez-Triguero, M. Moliner and A. Corma, *Catal. Sci. Technol.*, 2016, **6**, 2796–2806.
67 X. Zhang, H. Zhou, Y. Ye, X. You, X. Zhou, S. Jiang, K. Liu and A. D. Chowdhury, *Inorg. Chem. Front.*, 2023, **10**, 6632–6645.
68 Y. Shu, D. Ma, L. Xu, Y. Xu and X. Bao, *Catal. Lett.*, 2000, **70**, 67–73.
69 C. H. L. Tempelman and E. J. M. Hensen, *Appl. Catal., B*, 2015, **176–177**, 731–739.
70 I. Vollmer, A. Mondal, I. Yarulina, E. Abou-Hamad, F. Kapteijn and J. Gascon, *Appl. Catal., A*, 2019, **574**, 144–150.
71 L. Zhang, R. Tu, G. Ren, Z. Li, S. Zhai, Y. Xu and T. Yu, *Chem. Eng. J.*, 2023, **458**(15), 141447.
72 Y. Fang, X. Su, G. Ren, X. Bai, W. Wu, G. Wang, L. Xiao and A. Yu, *J. Energy Chem.*, 2017, **26**, 768–775.
73 J. Song, Q. Miao, Y. Lv, Z. Wang, Y. Li, L. Wang, M. Dong, P. Wang, Z. Qin and W. Fan, *Microporous Mesoporous Mater.*, 2024, **364**, 112877.
74 D. Zhang, H. Liu, L. Ling, H. Zhang, R. Zhang, P. Liu and B. Wang, *Phys. Chem. Chem. Phys.*, 2021, **23**, 10988.
75 Z. Feng, X. Liu and C. Meng, *Appl. Surf. Sci.*, 2023, **236**, 157811.
76 Y. Ni, W. Zhu and Z. Liu, *J. Energy Chem.*, 2021, **54**, 174–178.
77 Z. Shi and A. Bhan, *Chem. Eng. J.*, 2023, **456**, 140867.
78 E. A. Uslamin, H. Saito, Y. Sekine, E. J. M. Hensen and N. Kosinov, *Catal. Today*, 2021, **369**, 184–192.
79 S. Müller, Y. Liu, F. M. Kirchberger, M. Tonigold, M. Sanchez-Sanchez and J. A. Lercher, *J. Am. Chem. Soc.*, 2016, **138**, 15994–16003.
80 R. Khare, D. Millar and A. Bhan, *J. Catal.*, 2015, **321**, 23–31.
81 X. Gong, M. Çağlayan, Y. Ye, K. Liu, J. Gascon and A. D. Chowdhury, *Chem. Rev.*, 2022, **122**, 14275–14345.
82 S. Ilias and A. Bhan, *ACS Catal.*, 2013, **3**, 18–31.
83 T. Li, S. H. Chung, S. Nastase, A. Galilea, Y. Wang, I. Mukhambetov, M. Zaarour, J. C. N. de Miguel, J. Cazemier, A. Dokania, L. Panarone, J. Gascon, L. Cavallo and J. Ruiz-Martínez, *Chem. Catal.*, 2023, **3**(6), 100540.
84 D. P. Serrano, J. M. Escola and P. Pizarro, *Chem. Soc. Rev.*, 2013, **42**, 4004–4035.
85 M. Albahar, C. Li, V. L. Zholobenko and A. A. Garforth, *Microporous Mesoporous Mater.*, 2020, **302**, 110221.
86 W. Dai, L. Zhang, R. Liu, G. Wu, N. Guan and L. Li, *ACS Appl. Mater. Interfaces*, 2022, **14**, 11415–11424.
87 M. A. B. Siddiqui, A. M. Aitani, M. R. Saeed and S. Al-Khattaf, *Top. Catal.*, 2010, **53**, 1387–1393.
88 S. Schallmoser, T. Ikuno, M. F. Wagenhofer, R. Kolvenbach, G. L. Haller, M. Sanchez-Sanchez and J. A. Lercher, *J. Catal.*, 2014, **316**, 93–102.
89 A. Liutkova, H. Zhang, J. F. M. Simons, B. Mezari, M. Mirolo, G. A. Garcia, E. J. M. Hensen and N. Kosinov, *ACS Catal.*, 2023, **13**, 3471–3484.
90 X. Li, M. Sun, R. J. Claire, L. Chen and B. Su, *Chin. J. Catal.*, 2013, **34**, 22–47.
91 M. Sun, S. Huang, L. Chen, Y. Li, X. Yang, Z. Yuan and B. Su, *Chem. Soc. Rev.*, 2016, **45**, 3479–3563.